J Mater Sci (2012) 47:4400–4409
DOI 10.1007/s10853-012-6294-5

Graphene oxide: the mechanisms of oxidation and exfoliation

Guilin Shao · Yonggen Lu · Fangfang Wu · Changling Yang · Fanlong Zeng · Qilin Wu

Received: 21 November 2011 / Accepted: 21 January 2012 / Published online: 9 February 2012

Abstract Graphene oxides (GOs) with large sheets and more perfect aromatic structure were prepared by a novel modified Hummers method. We demonstrated that the graphite did not need to be oxidized to such a deep degree as described in Hummers method because the space distance increased little when the oxidation proceeded to a certain extent and the obtained graphite oxides (GTOs) could be fully exfoliated to single layers with high thermal stability. The oxidation mechanism and chemical structure model of GO were proposed by analyzing the evolution of the functional groups with oxidation proceeded based on thermogravimetric analysis, Fourier transform infrared spectroscopy, X-ray photoelectron spectroscopy, and Raman spectroscopy. The layer spacing calculated by molecular dynamics simulations coincided with the X-ray diffraction results. Furthermore, the size distribution and thickness of GOs were also studied. The results confirmed that the GOs prepared by the modified method were fully exfoliated to uniform single layers, and this method may be important for efficient exfoliation of GTO to GO and large-scale production of graphene.

Introduction

Graphene, a one-atom thick two-dimensional crystal, has attracted tremendous attention for its unusual electronic properties and possible application in various fields because it was first split from graphite by a scotch tape [1–6]. Nevertheless, several of these applications are still not feasible because the large-scale production of unbroken pure graphene sheets remains challenging. Recently, graphene oxide (GO), which was prepared by chemically oxidizing graphite to graphite oxide (GTO) with strong oxidants and ultrasonic cleavage, has attracted much attention as a possible intermediate for manufacture of graphene in large volume. In addition, because of the large amount of oxygen-containing functional groups [7], GO shows excellent hydrophilicity, and is relatively easily dispersed in water and even in other solvents through further modification [8, 9], making it easier to handle, functionalize, transport, and deposit than native graphene.

As a matter of fact, GTO was prepared as early as 1859 by Brodie [10] for ascertaining carbon atomic weight of graphite. Then Staudenmaier [11] and Hummers [12] proposed their own methods that improved experiment security and reduced formation of poisonous gas. Since then, oxidation of graphite has not drawn much attention until recently it was taken as a promising route for mass production of graphene by further processes of exfoliation and reduction [13]. Some modifications have been performed to the oxidation process based on Hummers method [14, 15]. However, the reaction time was still long. Additionally, few reports have discussed what degree the graphite should be oxidized to bound for efficient exfoliation to single layers, i.e., GO, and breaking the aromatic structure as slightly as possible. Eda and his co-worker demonstrated that graphite can be exfoliated into individual sheets via mild oxidation followed by intercalation. However, the exfoliation of partially oxidized and intercalated graphite was less efficient compared to GTO prepared through the modified Hummers method [16]. Ang reported an approach to obtain

G. Shao · Y. Lu (✉) · F. Wu · F. Zeng · Q. Wu
State Key Laboratory for Modification of Chemical Fibers and Polymer Materials, Donghua University, Shanghai 201620, China
e-mail: yglu@dhu.edu.cn

C. Yang
College of Chemistry, Chemical Engineering and Biotechnology, Donghua University, Shanghai 201620, China

mildly oxidized graphene sheets, coupled with a high monolayer yield (~90%) based on the intercalation and exfoliation of GTO sediments with tetrabutylammonium ions at the cost of a long process for more than 2 days [17].

Exfoliation of GTO depends on how weak the layers attract to each other and how strong the reaction between the layers and the solvent, i.e., on its layer spacing and the functional groups formed on the sides of the sheets, where the layer spacing is thought to be related to but not proportional to the oxidation degree. In consideration of reduction, the oxidation degree must be controlled as slight as possible on the promise that single layer GO can be obtained from the GTO. However, the oxidation mechanism and the structure of GTO are still elusive due to its nonstoichiometric structure and strongly hygroscopic property. Lerf and Klinowski proposed a structural model for GTO prepared by Hummers, according to which GTO contained two kinds of randomly distributed regions: aromatic regions with unoxidized benzene rings and regions with aliphatic six-membered rings. The relative size of the two regions depended on the degree of oxidation, with hydroxyl and epoxy groups located on the interior of GTO and carboxyl (COOH) groups at the edges of layers [18]. Wilson et al. [19] found that this model was consistent with their observations based on transmission electron microscopy imaging and diffraction. The layers remained planar with some corrugation that was distorted by the oxygen groups. However, the influence of layer spacing on exfoliation was not discussed. Szabo and his coworkers investigated the evolution of surface functional groups in a series of progressively oxidized GTOs by Brodie method and proposed a structural model by reviving the model of Scholz. The model exhibited a carbon network consisting of two regions: trans-linked cyclohexane chairs and ribbons of flat hexagons with C=C double bonds decorated with functional groups such as tertiary OH, 1,3-ether, ketone, quinone, and phenol [20]. It seemed that the aromatic structure of graphite was completely destroyed by oxidation of Brodie method. Therefore, Hummers method is more suitable for preparing graphene. Although it was believed that the functional groups resulted in the layer loosening of graphite, which was demonstrated by atomic-force microscopy and X-ray diffraction (XRD), much work remained for the mechanism that results in the development of GO from graphite.

In this study, GOs were prepared by the newly modified Hummers methods and Hummers method to investigate the oxidation mechanism and chemical structure of GO. Molecular dynamics (MD) simulation was employed to simulate the evolution of interlayer distance for oxidized graphite sheets. As few studies about GO colloid solution had been made that showed some potential applications, the properties of the derived GO, including sheet size distribution, the saturated concentration, and delamination, were also investigated.

Experimental

Preparation of GOs and GTOs

At first, GTO was prepared by Hummers method following the procedure mentioned in ref. [21]. At low-temperature stage, 5 g of graphite (purity degree $\geq$ 99.5%, ~30 μm) was mixed with 115 mL concentrated H_2SO_4 and 2.5 g $NaNO_3$ in ice bath for half an hour. 15 g $KMnO_4$ was slowly added into the mixture within 1 h to keep the temperature of the mixture not exceeding 5 °C. The mixture was then kept stirred for 1 h. At intermediate temperature stage, the mixture was heated to 35 °C and kept stirring for 2 h. During high-temperature stage, dropwise addition of 230 mL distilled water and external heating was introduced to maintain the reaction temperature at 98 °C for 15 min. Finally, the oxidation reaction was terminated by the addition of 700 mL distilled water and 50 mL 30% H_2O_2 solution. The resultant solid product was repeatedly washed with 5% HCl aqueous solution and then distilled water and dried at 60 °C under vacuum for 12 h. The GTO prepared by this method was named as HGTO.

GTO was also prepared by the following method modified on the basis of the Hummers method. After the same reaction at low temperature as in Hummers method, the mixture was heated up to 60 °C and held for 30 min, then 230 mL distilled water was added into the mixture that was heated for additional 30 min at the same temperature. Finally, the oxidation was terminated and the resultant was washed as in Hummers method. The GTO synthesized under this oxidation conditions was named as MGTO1. Similarly, the GTOs prepared at 60 °C for 15 min, 45 °C for 1 h, and 30 °C for 1 h were named as MGTO2, MGTO3, and MGTO4, respectively.

About 7.5 mL filtered cake of the rinsed GTOs was ultrasonicated in 50 mL water with power of 100 W for 15 min, let the solutions precipitate for 24 h and the deposits are discarded obtaining GO aqueous solution with the concentration of 2.5–4.5 mg/mL. The samples in the state of GO aqueous solution (dry GO included) were named as HGO, MGO1, MGO2, MGO3, and MGO4 corresponding to HGTO, MGTO1, MGTO2, MGTO3, and MGTO4, respectively.

Characterizations

The distribution of the GO sheet size was measured on a Malvern Nano-ZS Particle Size & Zeta Potential Analyzer of UK.

Typical tapping-mode atomic-force microscopy (AFM) images for GO were obtained on a Veeco-Nano scope IV AFM. Samples for AFM measurement were prepared by depositing diluted aqueous GO colloidal solution onto freshly cleaved micas and drying at 60 °C under vacuum for 12 h.

XRD patterns for the raw graphite, the GTOs, and dried GOs from the solutions were recorded at a D/Max-2550 PC X-ray diffractometer of Japan with CuKa ($\lambda = 0.1542$ nm) radiation, from which the layer distances were calculated.

Because ultrasonication had little influence on the thermal stabilities and chemical compositions of GO, the following measurements were done on GTOs instead of GOs.

Thermal tests were preformed on a 209 F1 Iris synchronous thermogravimetric analysis (TGA) in nitrogen atmosphere with a heating rate of 10 °C/min from 30 to 900 °C.

The Fourier transform infrared spectroscopy (FTIR) spectra have been recorded in the range 4000–500 cm^{-1} using the KBr pressed pellet technique, with a NEXUS-670 analytical FTIR Spectrometer of America. The potassium thiocyanate (KSCN) was used as calibration.

The atomic percentage of different elements and functional groups present probed by an AEI XSAM800 X-ray photoelectron spectroscopy (XPS) of UK was calculated from the survey spectra by considering the integrated areas of the main XPS peaks of the elements that were found.

Raman spectra were recorded from 200 to 2,000 cm^{-1} on a Renishaw Via-Reflex Confocal Raman Microprobe of England using a 532 nm excitation.

Details of the simulations

For the simulations, we used the Forcite module of Accelrys Materials Studio 5.5 that was developed by Neo-Trident Technology Ltd. with universal force field and atom-based electrostatic and van der Waals summation methods at the ultra-fine level of quality. The MD simulations were run with the starting temperature set at 298 K and NVE ensemble in 1 fs steps for 5.0 ps at a time (5,000 steps).

Results and discussion

Chemical structure of GO and the oxidation mechanism

Because the oxygen functional groups of GTOs decomposed on heating, their thermal stability could be directly demonstrated by the TGA curves. Figure 1 shows that samples MGTO2, MGTO3, and MGTO4 had a higher thermal stability, with a slight weight loss less than 10% before 600 °C followed by a sharp weight loss of 20–25% in the range of 700–820 °C and remains more than 60 wt% at 900 °C, whereas the decomposition law of MGTO1 was consistent with HGTO that lost about 30–40 wt% at 230 °C, kept relatively stable till 660 °C and remained 20–25 wt% at 900 °C. The sharp weight loss at 230 °C for the last two samples might be ascribed to decomposition of some unstable groups formed due to over oxidation. Apparently, MGTO2–4 were much stable than MGTO1 and HGTO, meaning a more perfect structure with a lower oxidation degree. Because the similar thermal decomposition laws of MGTO2, MGTO3, and MGTO4 suggested that the structure of them was similar, the following measurements were done only on MGTO3.

The FTIR spectra were used to further investigate the chemical structure of GTO samples (Fig. 2). The relative amount of the functional groups except for phenolic (OH) groups could be estimated according to the peak intensity normalized by the calibration KSCN. For HGTO and MGTO1, the spectra of HGTO and MGTO1 are similar, in which the peak at 3,424 cm^{-1} attributed to OH stretching vibration and the peak at 1,621 cm^{-1} to OH bending vibration indicate the existence of adsorbed water molecules and structural OH groups [22–24]. The next relatively strong bands at 2,920 cm^{-1} and 2,851 cm^{-1} may refer to the C–H stretching vibration of CH_2 groups. Besides, a band at 1,721 cm^{-1} might be related to not only the C=O stretching motions of COOH groups situated at the edges and defects of GO lamellae but also that of the ketone or quinone groups. Therefore, the band at 1,400 cm^{-1} ascribed to the OH deformation vibration of COOH groups can be used to evaluate the amount of COOH groups. The bands at 1,242 cm^{-1} and 1,119 cm^{-1} are corresponded to C–O–C and OH [25, 26]. For MGTO3, the spectrum is

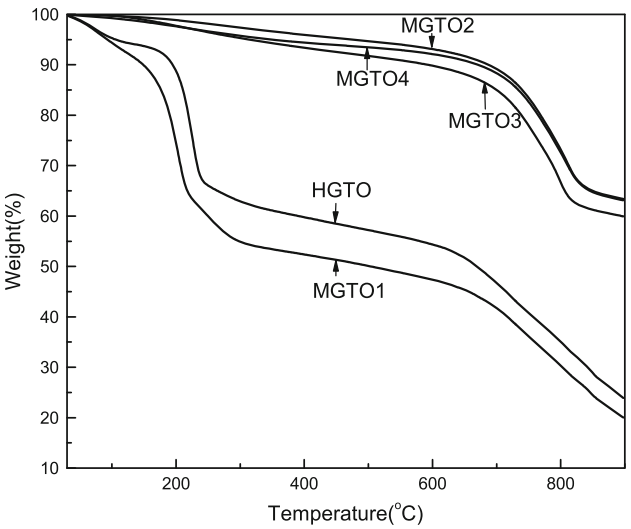

Fig. 1 TGA curves of HGTO, MGTO1, MGTO2, MGTO3, and MGTO4 with a heating rate of 10 °C/min in nitrogen

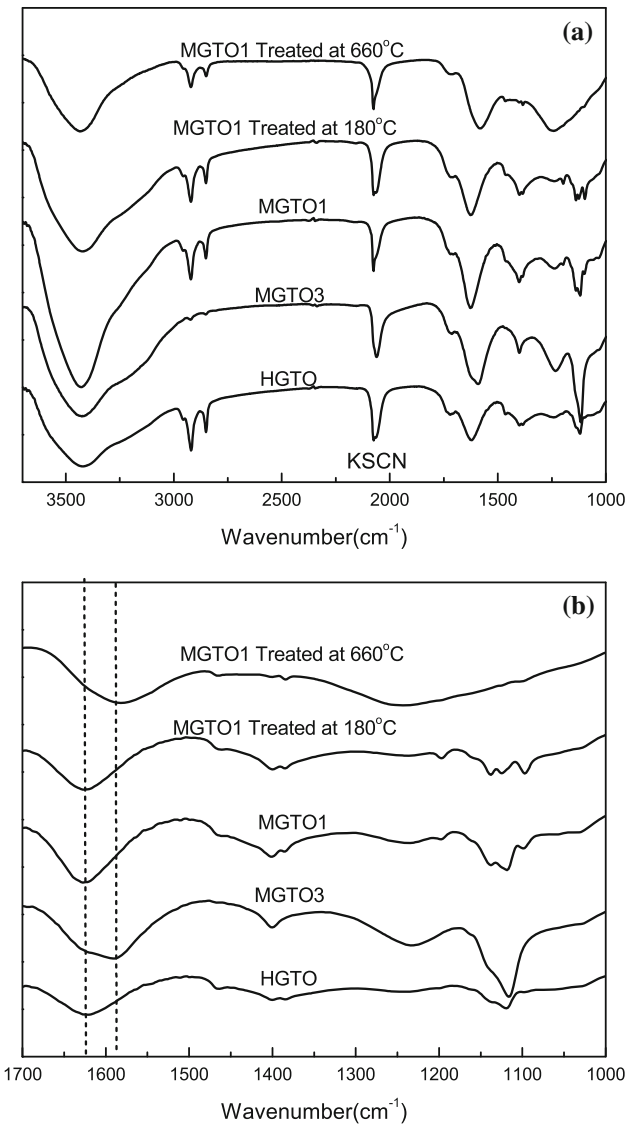

Fig. 2 **a** FTIR spectra of HGTO, MGTO3, MGTO1, and MGTO1 treated at 180 and 660 °C. **b** Magnified FTIR spectra with the wavenumber ranges from 1,700 to 1,000 cm^{-1}

different from the other two samples. The CH_2 peaks for MGTO3 almost cannot be observed, indicating that there are few CH_2 groups on MGTO3. The peak near 1,700–1,550 cm^{-1} widens and moves to 1,586 cm^{-1} that reflects the presence of unoxidized aromatic regions [22, 27]. This shows that the aromatic structure was seriously destroyed with the extension of reaction time and rise of oxidation temperature. Besides, the peak intensity of COOH groups at 1,400 cm^{-1} is lower than MGTO1 but both are stronger than HGTO.

It is shown from Fig. 2a that the spectrum of MGTO1 almost has no change after treated at 180 °C. However, after treated at 660 °C, the COOH and OH peaks disappear while the C–O–C peak increases. Furthermore, a new peak appears at 1,586 cm^{-1} reflecting the carbon skeletal vibration of graphene sheets just like MGTO3. This observation confirms that the first mass loss point at 230 °C for HGTO and MGTO1 in TGA curves mainly ascribed to the full decarboxylation of carboxyl groups and loss of part of OH after heat treatment. In addition, the other part of the OH dehydrated and converted to C–O–C groups.

Because it was difficult to fully dehydrate a GTO sample, XPS was used as a complement to analyze the relative amount of carbon, oxygen, and functional groups with the exception of water, and the results were shown in Table 1. The C/O atom ratio was about 2.33, 2.28, and 2.25 for HGTO, MGTO1, and MGTO3, respectively, which indicates that the oxidation degree of three samples was similar. Such a large amount of oxygen could not only exist on the edges of graphene sheets. Therefore, it was believed that the oxygen-containing functional groups were inserted into carbon skeleton during the oxidation process. The high-resolution C 1s spectra of three samples presented in Fig. 3 showed existence of following functional groups: graphitic carbon C=C (284.8–284.6 eV), epoxy/hydroxyls C–O (286.4–286.6 eV), ketone/quinone C=O (287.2–288.0 eV), and carboxylates O–C=O (288.2–289.3 eV) according to the reported peak-fitting methods [28, 29]. From Table 1 it was noted that there are more C=C and C–O groups but less O–C=O and C=O groups on MGTO3 than the other two samples, which was consistent with FTIR results.

Raman spectroscopy is a widely used tool for the characterization of carbon products. A universal observation is that higher disorder in graphite leads to a broader G-band, as well as to a broad D-band of higher relative intensity compared to that of the G-band [30]. The I_D/I_G is a measure of the disorder, as expressed by the sp^2/sp^3 carbon ratio [31]. That is, the I_D/I_G and full width at half maximum (FWHM) are related to the sample defects created by the attachment of functional groups on the carbon and indicative of the integrity of the aromatic structure. Figure 4 shows the Raman spectra of the as-prepared

Table 1 The amount of elements and functional groups for HGTO, MGTO1, and MGTO3

Samples	C (at.%)	O (at.%)	C/O	C=C (at.%)	C–O (at.%)	C=O (at.%)	O–C=O (at.%)
HGTO	70.00	30.00	2.33	49.15	43.55	5.31	2.00
MGTO1	69.47	30.53	2.28	49.95	42.87	5.82	1.36
MGTO3	69.27	30.73	2.25	51.00	46.28	2.38	0.33

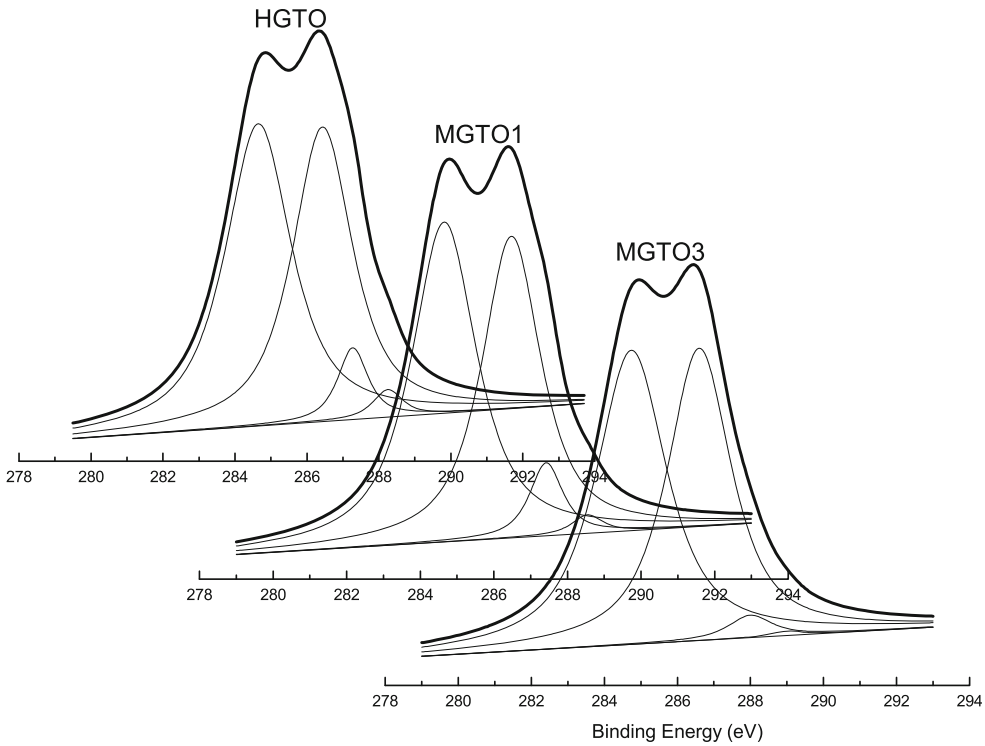

Fig. 3 High-resolution C 1s spectra XPS of HGTO, MGTO1, and MGTO3

GTOs with D-band at 1,351 cm^{-1} and a G-band at 1,590 cm^{-1} with different intensity and shape. The ratios of I_D/I_G and FWHMs are listed in Table 2, showing that the I_D/I_G of MGTO3 is lower than those of the other two GTOs, whereas the D-band and G-band of the other two GTOs are wider than MGTO3. This suggests that the aromatic structure of MGTO3 was more perfect than the others. The Raman spectra of the GTOs after treating at 1,200 °C also contain both G-band and D-band, however, with decreased I_D/I_G ratios and narrowed peaks compared with that in GTOs. This change is attributed to the decreased defect concentration present in GTOs after heat treatment that may be due to the recovery of hexagonal network of carbon atoms. In addition, the I_D/I_G of MGTO1 after heat treatment is lager than that of MGTO3 after heat treatment, which also indicated that the aromatic structure of MGTO3 was more perfect than MGTO1 that was consistent with TGA and FTIR results.

Based on above analysis, the oxidation mechanism of graphite sheets was deduced. A graphene sheets with two inherent defects as the initial source (Fig. 5a), after reacting with reagents less than 5 °C, the graphite converted to

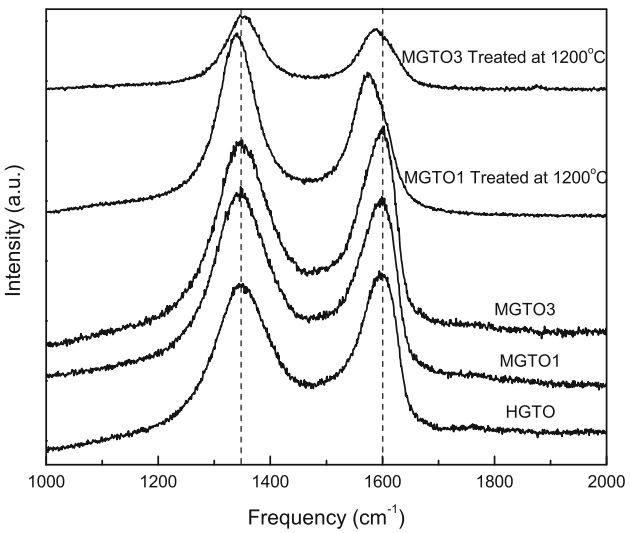

Fig. 4 Raman spectra of HGTO, MGTO1, MGTO3, MGTO1 treated at 1,200 °C, and MGTO3 treated at 1,200 °C

Table 2 Raman data of HGTO, MGTO1, MGTO3, MGTO1 treated at 1,200 °C, and MGTO3 treated at 1,200 °C

Sample	D-band peak		G-band peak		I_D/I_G
	Raman shift (cm^{-1})	FWHM (cm^{-1})	Raman shift (cm^{-1})	FWHM (cm^{-1})	
HGTO	1,351	129	1,590	70	1.77
MGTO1	1,351	125	1,590	73	1.78
MGTO3	1,351	123	1,590	69	1.70
MGTO1#	1,340	85	1,575	67	1.61
MGTO3#	1,352	77	1,588	65	1.45

I_D/I_G is the integrated intensity ratio of D-band and G-band

FWHM is the full width at half maximum

MGTO1# MGTO1 treated at 1,200 °C, *MGTO3#* MGTO3 treated at 1,200 °C

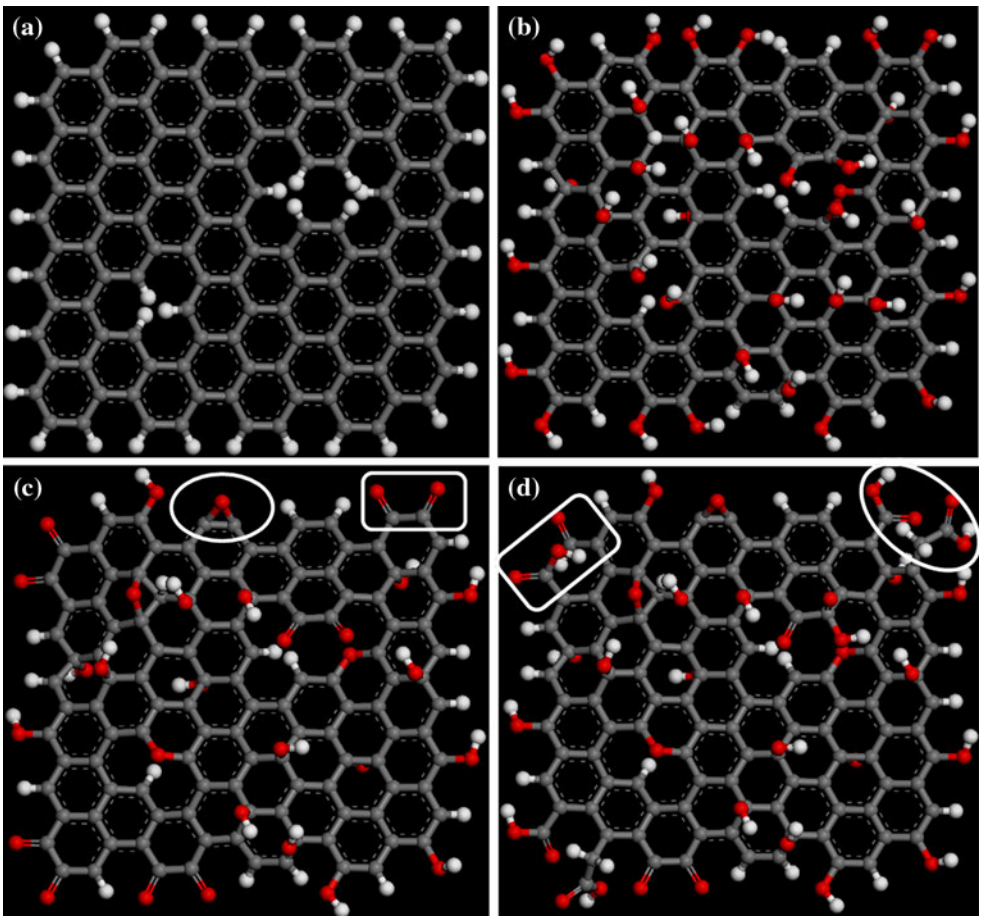

Fig. 5 The oxidation mechanism model of graphite sheets

graphite intercalation compound (GIC) of sulfuric acid [32], which made the graphite more reactive to oxidation but did not change the graphene structure much. The oxidation would be initiated on the active positions of the graphene sheets, i.e., on the edges and imperfect regions. During followed oxidation process, a large number of phenolic groups produced first at the edges and defects then on the basal plane of graphene sheets under strong oxidation of $KMnO_4/H_2SO_4$. Simultaneously, the double bonds that attached to these chemical reaction points were transformed into single bonds (Fig. 5b). With oxidation proceeded, on one hand, part of phenolic groups might condense to form C–O–C (ether) linkages (Fig. 5c, oval). On the other hand, a small proportion of phenolic groups at the edges or defects were oxidized to two adjacent ketone groups, that is, the phenolic groups were oxidized to quinone groups (Fig. 5c, square). Subsequently, the ketone groups converted to COOH (Fig. 5d, square). If it was carboxyl or carbonyl groups that adjacent to COOH groups, owning to the electrophilic effect and anionic mechanism, the COOH groups decarboxylated easily and C–C bond between them cleaved. If there are three carbons that attached to hydrogen at the edges in one benzene ring were oxidized, then one CH_2 could form (Fig. 5d, oval). Of course, there were still some ketone and quinone groups left. Hence, the amount of oxygen functional groups except for phenolic groups was increased as the oxidation proceeded.

What is more, the reactions of carbon atoms in a graphene layer with other species could lead to the loss of atoms and hence to defects. Oxidation was the most common one, for example, in a strong oxidizing mixture ($KMnO_4/H_2SO_4$). Although the high inertness of graphene (apart from edge positions that are highly reactive) only allowed a very limited number of possible reactions at room temperature, with reaction time and temperature rise, more defects formed, which could lead to lower thermal stability of the samples. Therefore, this was another reason why the thermal stability of MGTO3 was higher than HGTO and MGTO1, as observed in TGA.

According to the oxidation mechanism and analysis described earlier, a structure model of the GOs was

proposed by revising the model of Lerf et al. [18]. The aromatic structure of the GOs was not perfect due to the intrinsic and extrinsic defects especially vacant defects. Phenolic groups and ethers distributed randomly above and below the sheets, while ketones and quinones together with COOH could be formed at the defects and edges, CH_2 could also produced where COOH groups were decarboxylated, and C–C bonds were cleaved. More C=C and phenolic groups would be converted to C–C and C–O–C, C=O, O–C=O with the formation of CH_2 groups when the oxidation time and temperature were increased.

Evolution of layer spacing from graphite to GTO and GOs

As a way to "loosen" the graphitic layers for easy exfoliation, the oxidation was supposed to make the layer spacing enlarge rather than more oxygen groups produce. The powder XRD patterns of HGO, MGO1, MGO3, and MGTO1 together with that of raw graphite are shown in Fig. 6. The pattern of the raw graphite shows a very strong (002) peak at 26.54° for a typical graphitic structure with a layer spacing of 0.334 nm. However, after oxidation, it is obvious that the characteristic graphitic peak completely disappears and a new diffraction peak appears at about 11.3° for MGTO1 with a layer spacing of 0.78 nm. The re-aggregated GOs, including HGO, MGO1, MGO3, also show a similar diffraction peak at about 10.6–11.0°, corresponding to layer spacing of 0.80–0.83 nm, respectively, which indicates that the layers of the GOs stacked again during drying. The results indicate that the layer spacing did not increase any more when the oxidation proceeded to a certain extent. So even if the reaction time was shorter

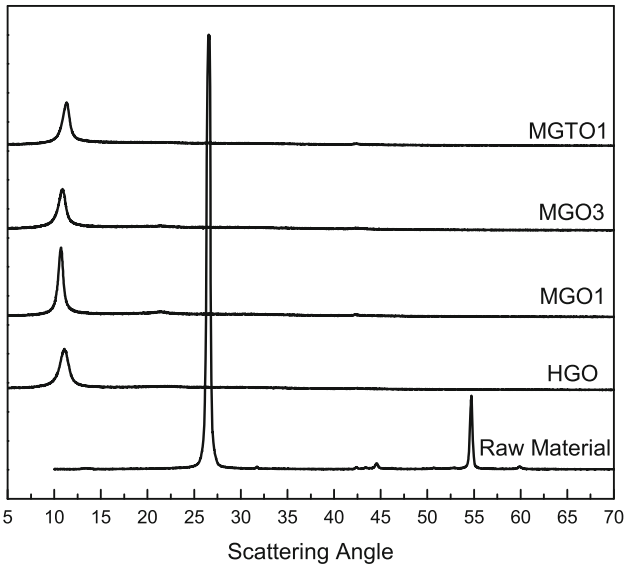

Fig. 6 The XRD spectra of raw graphite, HGO, MGO1, MGO3, and MGTO1

and the oxidation temperature was lower, the space distance of MGO3 could also increase to the same as that of HGO. Anyway, the oxygen functional groups attached on both sides of the graphene sheets and the arising atomic scale roughness to the originally atomically flat graphene sheets [33] were responsible for the enlarged layer spacing, which can be simulated by MD simulations.

Figure 7 shows two-layer graphene sheets (the number of carbon atoms, $N_C = 702$) and two-layer GO sheets ($N_C = 702$ and the number of oxygen atoms, $N_O = 304$) suspended in vacuum with two mono-vacancy defects and one di-vacancy defect on each sheet. The oxygen atoms

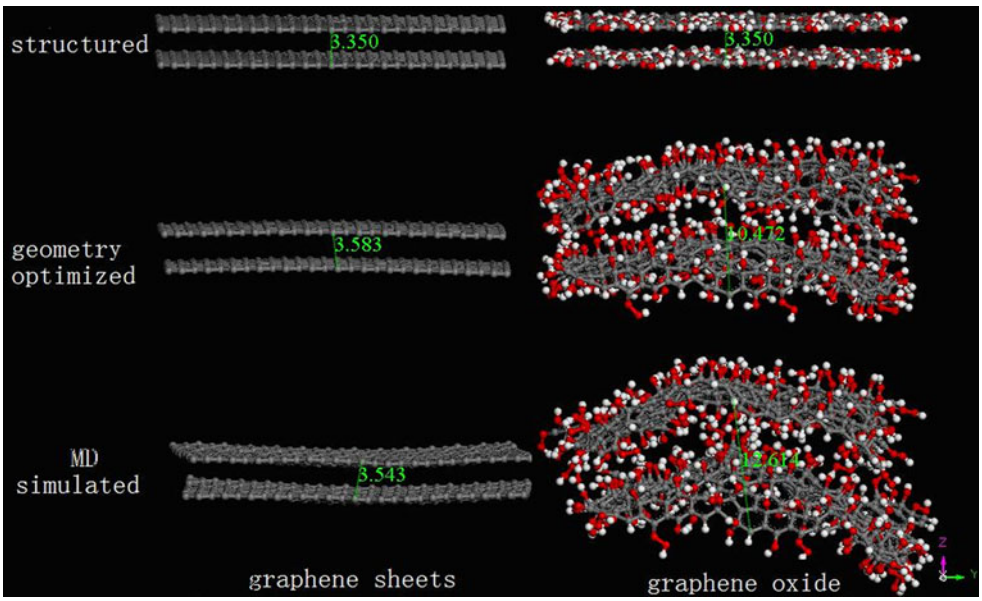

Fig. 7 Molecular models of two-layer graphene sheets and graphite to GTO transition

and functional groups were added to the GO sheets according to the analytic results by XPS, i.e., 5 carboxyl groups (O–C=O) and 30 quinone groups (C=O) distributing at the edges and defects, 30 epoxy groups (C–O–C) on the basal planes, 204 phenolic (OH) groups everywhere, and hydrogen atoms at all the unsaturated sites of the sheets. It is noted that the interlayer distance of graphene sheets increases a little after geometry optimization and MD simulation, while that of the GO sheets remarkably increases from 0.335 to 1.2 nm with the sheets severely corrugated. The results almost coincided with that calculated from XRD.

Dispersion and the solutions

The colloidal suspension solutions of HGO, MGO1, and MGO3 were prepared by dispersing them in water with a concentration of 5 mg/mL after sonicating at 100 W for 30 min, let the solutions stand for 24 h, and then removed the deposits to separate the exfoliated GO sheet from the nonexfoliated sheets. After calculating, the saturated concentrations of the three samples were 3.97, 2.83, and 4.56 mg/mL, respectively. Similarly, the colloidal suspension solutions of the three samples were prepared with a concentration of 0.5 mg/mL, then did the same as above, the delamination ratios of the three samples were 90.0, 50.2, and 95.8%, respectively. Therefore, MGO3 could be dispersed and delaminated more easily than MGO1 and HGO even though its oxidation time was shorter and the oxidation temperature was lower. These colloid solutions were found to be stable for several months in which Tyndall effect was observed.

AFM is one of the powerful tools to investigate the exfoliation rate and thickness of graphitic flakes (Fig. 8). It can be found from Fig. 8 that the mean thickness is 0.9–2.3, ~1.0, and ~1.0 nm for HGO, MGO1, and MGO3

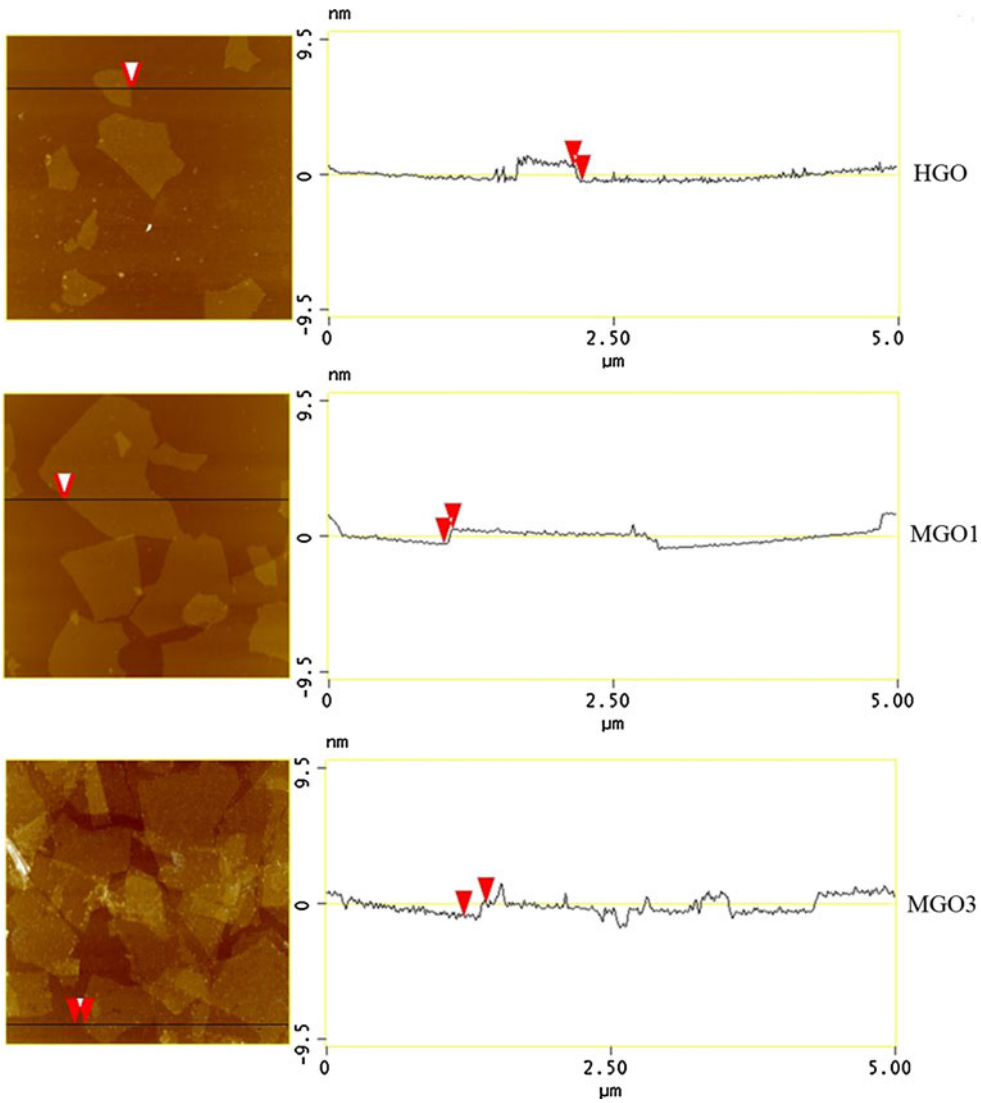

Fig. 8 AFM images and layer height profiles of HGO, MGO1, and MGO3

sheets, respectively which indicates that MGO1 and MGO3 are thinner than the HGO. According to the previous studies on statistical evaluation, the mean thickness of a single GO sheet was suggested to be ~1.0 nm [34–37]. The conclusion is that MGO1 and MGO3 could be regarded as full exfoliation to monolayer and the yield was 100%, whereas the HGO sheets existed as single or few layers. This suggests that it was not necessary to prepare GTO samples with such high temperature and long time.

As the particle size measurement on this instrument was based on the assumption that the particles were spherical, the instrument was unable to give the absolute size of graphene sheets. Nevertheless, the measurements obtained provided a means of testing size distribution. From Fig. 9 it can be found that the size distributions are approximately Gaussian, the size distribution of MGO3 varies from 300 to 690 nm, whereas for MGO1, the size distribution varies from 270 to 690 nm and the average sizes are 1,456, 1,447, and 1,520 nm for HGO, MGO1, and MGO3, respectively. The results indicated that MGO3 could provide more uniform big layers.

Based on the chemical structure analysis and dispersion properties described in the preceeding, it was considered that HGTO and MGTO1 were a little over oxidized. Even though MGTO3 was synthesized at lower temperature for shorter time, it still could be fully exfoliated. Furthermore, the thermal stability was higher and the layers were more big and uniform. In addition, the aromatic structure of MGO3 was more perfect, which was more suitable and easy for reduction to graphene. So the oxidation degree should be controlled as slight as possible, as long as the layer spacing is enlarged enough to obtain GOs with more perfect aromatic structure.

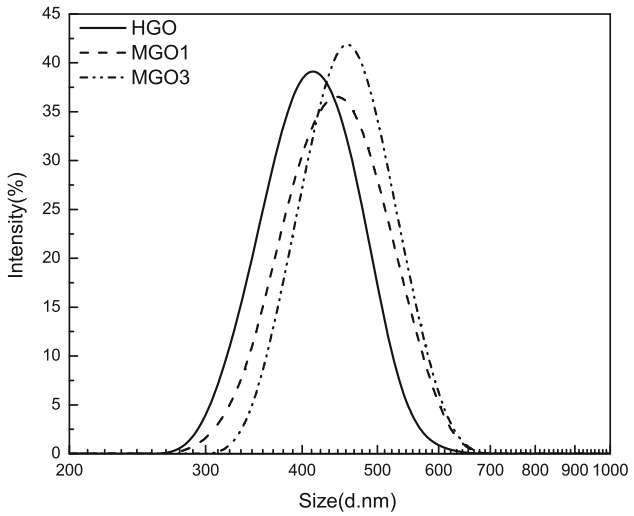

Fig. 9 The size distributions of HGO, MGO1, and MGO3 sonicated at 100 W for 15 min with a same concentration

Conclusion

In conclusion, GOs successfully prepared by a modified Hummers method with shorter time and lower oxidation temperature exhibited larger sheets and higher thermal stability with a weight remain more than 90 wt% at 600 °C and 60 wt% at 900 °C, 36 wt% higher than that obtained by Hummers method. The oxidation mechanism and chemical structure model of GO were proposed. During oxidation process, phenolic groups formed firstly not only at the edges but also on the basal plane of graphene sheets. With further development of oxidation, part of phenolic groups converted to C–O–C or quinone groups, subsequently quinone was transformed into ketone groups and O–C=O accompanied with the formation of CH_2 groups, which destroyed the aromatic structure of GO. The chemical structure model of GO was proposed by revising Lerf and Klinowski's model via increasement of C=O and CH_2 groups at the edges and defects of GO. We found that the space distance did not increase any more when the oxidation proceeded to a certain extent. So the oxidation degree should be controlled as slight as possible as long as the layer spacing is enlarged enough so that GOs prepared with more perfect aromatic structure. The layer spacing calculated by MD simulations coincided with the experimental measurement.

Acknowledgements The financial support of this work by the National Basic Research Program of China ("973 Program", Grant Nos.: 2011CB605602 and 2011CB605603) and the Cultivation Fund of the Key Scientific and Technical Innovation Project, Ministry of Education of China are gratefully acknowledged.

References

1. Liang M, Zhi L (2009) J Mater Chem 19:5871
2. Geim AK (2009) Science 324:1530
3. Novoselov KS, Geim AK, Morozov SV, Jiang D, Zhang Y, Dubonos SV, Grigorieva IV, Firsov AA (2004) Science 306:666
4. Chen X, He Y, Zhang Q, Li L, Hu D, Yin T (2010) J Mater Sci 45:953. doi:10.1007/s10853-009-4025-3
5. Liu Y, Chen Z, Yang G (2011) J Mater Sci 46:882. doi:10.1007/s10853-010-4829-1
6. Zhang Y, Pan C (2011) J Mater Sci 46:2622. doi:10.1007/s10853-010-5116-x
7. Kovtyukhova NI, Ollivier PJ, Martin BR, Mallouk TE, Chizhik SA, Buzaneva EV, Gorchinskiy AD (1999) Chem Mater 11:771
8. Wang Y, Xie L, Sha J, Ma Y, Han J, Dong S, Liu H, Fang C, Gong S, Wu Z (2011) J Mater Sci 46:3611. doi:10.1007/s10853-011-5277-2
9. Yoon S, In I (2011) J Mater Sci 46:1316. doi:10.1007/s10853-010-4917-2
10. Brodie BC (1859) Philos Trans R Soc London 149:249
11. Staudenmaier L (1898) Ber Dtsch Chem Ges 31:1481
12. Hummers WS, Offeman RE (1958) J Am Chem Soc 80:1339
13. Su C, Xu Y, Zhang W, Zhao J, Liu A, Tang X, Tsai C, Huang Y, Li L (2010) ACS Nano 4:5285

14. Zhang L, Li X, Huang Y, Ma YF, Wan XJ, Chen YS (2010) Carbon 48:2367
15. Marcano DC, Kosynkin DV, Berlin JM, Sinitskii A, Sun ZZ, Slesarev A, Alemany LB, Lu W, Tour JM (2010) ACS Nano 4:4806
16. Eda G, Ball J, Mattevi C, Acik M, Artiglia L, Granozzi G, Chabal Y, Anthopoulos TD, Chhowalla M et al (2011) J Mater Chem 21:11217
17. Ang PK, Wang S, Bao Q, Thong JTL, Loh KP (2009) ACS Nano 3:3587
18. Lerf A, He H, Forster M, Klinowski J (1998) J Phys Chem B 102:4477
19. Wilson NR, Pandey PA, Beanland R, Young RJ, Kinloch IA, Gong L, Liu Z, Suenaga K, Rourke JP, York SJ, Sloan J (2009) ACS Nano 3:2547
20. Szabó T, Berkesi O, Forgó P, Josepovits K, Sanakis Y, Petridis D, Dékány I (2006) Chem Mater 18:2740
21. Rafiq R, Cai DY, Jin J, Song M (2010) Carbon 48:4309
22. Lian PC, Zhu XF, Liang SZ, Li Z, Yang WS, Wang HH (2010) Electrochim Acta 55:3909
23. Szabo T, Berkesi O, Dekany I (2005) Carbon 43:3186
24. Hontorialucas C, Lopezpeinado AJ, Lopezgonzalez JDD, Rojas-cervantes ML, Martinaranda RM (1995) Carbon 33:1585
25. Si Y, Samulski ET (2008) Nano Lett 8:1679
26. Murugan AV, Muraliganth T, Manthiram A (2009) Chem Mater 21:5004
27. Jeong H, Lee YP, Jin MH, Kim ES, Bae JJ, Lee YH (2009) Chem Phys Lett 470:255
28. Yue ZR, Jiang W, Wang L, Gardner SD, Pittman JCU (1999) Carbon 37:1785
29. Gardner SD, Singamsetty CSK, Booth GL, He G, Pittman CU (1995) Carbon 33:587
30. Kudin KN, Ozbas B, Schniepp HC, Prud'Homme RK, Aksay IA, Car R (2007) Nano Lett 8:36
31. Gómez-Navarro C, Weitz RT, Bittner AM, Scolari M, Mews A, Burghard M, Kern K (2007) Nano Lett 7:3499
32. Nakajima T, Mabuchi A, Hagiwara R (1988) Carbon 26:357
33. Shen JF, Hu YZ, Shi M, Lu X, Qin C, Li C, Ye MX (2009) Chem Mater 21:3514
34. Geng Y, Wang SJ, Kim JK (2009) J Colloid Interface Sci 336:592
35. Qian Y, Lu S, Gao F (2011) J Mater Sci 46:3517. doi: 10.1007/s10853-011-5260-y
36. Chen C, Yang Q, Yang Y, Lv W, Wen Y, Hou P, Wang M, Cheng H (2009) Adv Mater 21:3007
37. Stankovich S, Dikin DA, Dommett G, Kohlhaas KM, Zimney EJ, Stach EA, Piner RD, Nguyen ST, Ruoff RS (2006) Nature 442:282